Proceedings of 2021 IEEE
International Conference on Mechatronics and Automation
August 8 - 11, Takamatsu, Japan

Centerline Extraction Method for Virtual Vascular Model in Virtual Reality Interventional Training Systems

Peng Shi[1], Shuxiang Guo[1,2*]

[1]*Graduate School of Engineering*

Kagawa University
Hayashi-cho, Takamatsu, 761-0396, Japan
s19d503@stu.kagawa-u.ac.jp

Xiaoliang Jin[1] and Xinming Li[1]

[2]*Key Laboratory of Convergence Medical Engineering Sytem and Healthcare Technology, The Ministry of Industry and Information Technology, School of Life Science*
Beijing Institute of Technology
Haidian District, Beijing, 100081, China
**corresponding author: guo.shuxiang@kagawa-u.ac.jp*

Abstract **– Virtual reality (VR) interventional training systems are commonly used for vascular interventional surgery training. Compared with traditional training method, including using human cadavers, live animals and vascular phantom, VR interventional training has many advantages such as low training cost and variable training model. For virtual interventional radiology, simulating catheter interaction is a challenging work. Centerline of the vasculature is often used to detect the contact between blood vessel wall and surgical tools. In this paper, we proposed an improved centerline extraction method based on generalized rotational symmetry axis. The method discretizes the vasculature by a set of continuous cylindrical shapes. This discretization obtains an effective strategy for vasculature centerline extraction. In order to improve the algorithm efficiency, we use a pre-processing strategy to merge duplicate points and normal vector for vasculature mesh. This strategy turns the vasculature mesh into vasculature point cloud and reduced the number of calculation points. The performance of our method is experimentally validated.**

Index Terms – Centerline extraction, rotational symmetry axis, vasculature mesh, virtual interventional radiology, VR interventional training system.

I. INTRODUCTION

Coronary artery diseases, including the angina and myocardial infarction, is one of the main causes of mortality in developed countries [1-3]. Vascular interventional surgeries (VIS) are commonly used to treat these diseases because it has some advantages such as small incision to the healthy tissue, short recovery time, little postoperative, and good surgical outcomes [4-7]. However, vascular interventional surgeries require surgeon to be highly skilled at manipulating the surgical tools to reach lesion under the two-dimensional X-ray image guidance [8-10]. Traditional interventional training methods, including using human cadavers, live animals and vascular phantom, have many limitations such as expensive, risky and limited morphological models. Moreover, prolonged exposure to X-ray radiation during training procedure will cause a serious impact for the physicians' health [11].

Virtual reality interventional training systems were developed as a means of improving training and reducing the costs of education. Computer-based simulation of interventional surgeries provides a versatile solution and can virtually be reused infinite times on both common and rare cases. Moreover, patient-specific data can be used to reconstruct vasculature mesh, which helps surgeon to plan or rehearse preoperatively to evaluate and optimize the surgeries [12]. For VR interventional training system, one of the most challenging works is to simulate the dynamical behavior of guidewires and catheters. This requires accurate detection of contact between surgical tools and blood vessel wall. The commonly used method is to detect the contact by calculating the distance between the catheter and the centerline of the vasculature. Moreover, surgeons are usually interested in both the patient's vasculature and its centerline. The VR simulator need to provide the vasculature centerline to encourage operators to move both the catheter and guidewire along the centerline to reduce collision.

The centerline is closely related to curve skeletons. Blum's medial axis and its variants is designed to obtain centerline by capturing reflectional symmetries in a shape [13]. The medial axis of a 3D model is generally a non-manifold containing 2D sheets that are hard to store and manipulate. A 1D centerline is more useful in practice. Most commercial software use volume data to extract the vasculature centerlines, such as MeVisLab and MedCAD [14, 15]. However, when volume data is lacking, the software does not work very well. Sharf et al. proposed a method to compute a curve skeleton by a deformable blob grown form the "inside" of input cloud [16], and Tagliasacchi et al. achieve the extraction through a ROSA-based method [17]. These two methods are based on point cloud and can run under moderate amounts of missing data. Wang and Lee used iterative least squares optimization method that shrinks models and applies the thinning algorithm to extract 1D skeletons [18]. Au et al used implicit Laplacian smoothing with global position constraints to contract the mesh [19]. The contracted mesh is then converted into the curve skeleton while preserving the shape of the contracted mesh and the original topology. These methods aim to deal a series of shapes for a wider applicability. However, these methods are complicated and hard to be performed on vasculature mesh.

In this paper, we propose an improved centerline extraction method based on generalized rotational symmetry axis (ROSA) [17, 20]. Our method discretizes the vasculature mesh by a set of continuous cylindrical shapes. The centerline of vasculature is most appropriately thought of as a generalized rotational symmetry axis and it is composed of the center point for each cylinder. Moreover, our method can

978-1-6654-4098-1/21/$31.00 ©2021 IEEE

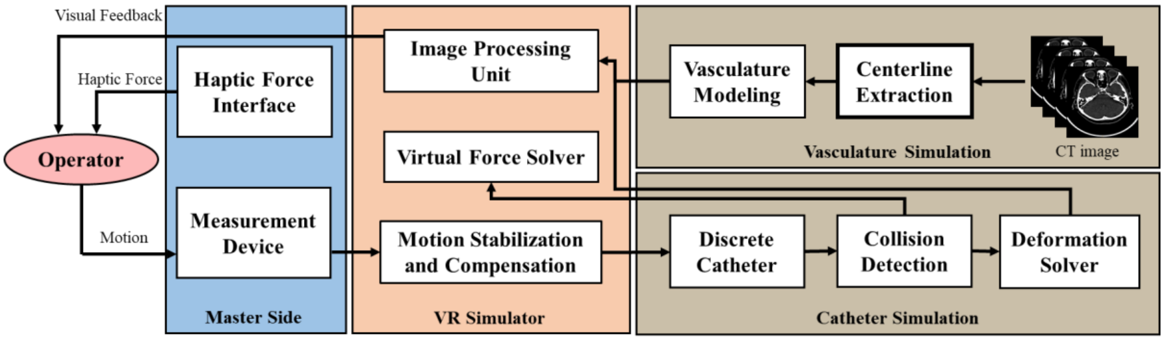

Fig. 1 An overview of our VR interventional training system.

effectively exploit orientation information to compute ROSA so as to compensate for the missing. Due to the vasculature mesh is made up of tiny triangle planes, the point cloud of vasculature mesh contains duplicate vertices. Our method uses a pre-processing strategy to merge duplicate vertices. Meanwhile, the plane normal vectors are converted to vertex normal vectors. This strategy turns the vasculature mesh into vasculature point cloud and reduced the number of calculation points. Therefore, the computational complexity of the algorithm is reduced.

The remainder of this paper is organized as follows. The proposed method is presented in Section II. In Section III, experiment is finished. Finally, the conclusion is given in Section IV.

II. Centerline Extraction Based on Rotational Symmetry Axis

An VR interventional training system includes the master side and VR simulator, as shown in Fig. 1. The master side is used to measure the motion of input catheter and provide the haptic force feedback. Our research group has developed the master side with haptic force interface which can provide high-accuracy force feedback [21-25]. VR simulator is used to provide the vasculature mesh and simulate the interaction between surgical tools and blood vessel wall. The vasculature modeling is based on curve skeleton and radius information from the patient vasculature information. Our research group proposed a vasculature reconstruct method [26-29], which can extract the vasculature information from computed tomography (CT) or magnetic resonance angiography images. For vasculature simulation, centerline extraction is the foundation of application. In this section, we introduce an improved centerline extraction method based on generalized rotational symmetry axis.

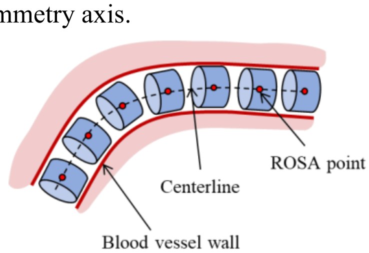

Fig. 2 A illustration for discretization of vasculature mesh. The rotational symmetry axis point forms the centerline.

A. *Discretization of Vasculature Mesh*

In generally circumstances, the cross-section of the blood vessel can be considered as a circular shape. The blood vessel can be approximated as the cylindrical tube. This cylindrical tube can be discretized as a set of continuous small cylindrical shapes, as shown in Fig. 2. Thus, the rotational symmetry axis from these small cylindrical shapes form the centerline of the blood vessel. For each small cylindrical shape, the center point of shape is lies on the centerline, and the radius of cylinder is the radius of blood vessel. We define a cutting plane through the center point of cylindrical shape and the normal of this plane is same as centerline. The subset S contains all the vertices for this cutting plane, and the center point is defined as $c=(p_{cp},\ n_{cp})$ with position p_{cp} and normal n_{cp}. This point is called ROSA point which is most rotationally symmetric about S.

Based on the above assumptions, we can obtain that the angle between the normal n_{cp} and the normal of other vertexes in subset S is always same, and this consistent with the notion of rotational symmetry. Moreover, the sum of distances between the position p_{cp} and the line extensions of the vertexes normal in subset S is minimum. The definition is illustrated in Fig. 3.

B. *Centerline Extraction via Rotational Symmetry Axis*

We need use planar cuts over the vasculature mesh to search the ROSA point. Let v_i be a vertex in vasculature. Suppose a cutting plane φ_i through the point v_i with normal n_i, and the subset S_i is formed by the vertexes which are close to cutting plane φ_i within a distance less than a threshold δ. In this research, we set $\delta=0.025L$, where L is

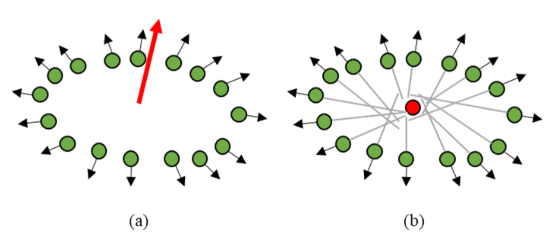

Fig. 3 The definition of rotational symmetry axis for a subset S. (a) The normal minimizes sum of angular variations with the vertex normal in S. (b) The position minimizes sum of projected distances to the normal extensions.

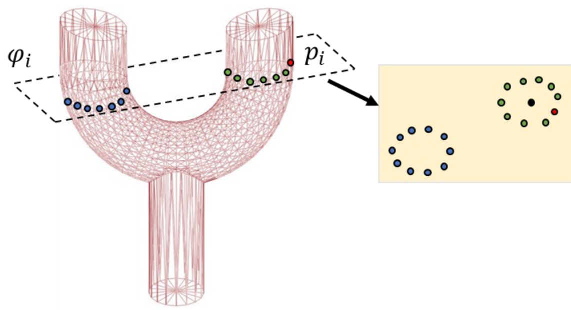

Fig. 4 The cutting plane for a vasculature mesh. The optimal cutting plane and relevant neighbourhood points (green points) anchored at a point sample (red point).

the bounding box diagonal of the vasculature mesh. Moreover, the cutting plane may through multiple shapes, as shown in Fig. 4. Thus we use k-means method to further identify the points close to the cutting plane φ_i, a relevant neighbourhood N_i of point cloud samples. In order to avoid a full-fledged clustering problem, N_i is anchored at v_i, i.e., $v_i \in N_i$. Therefore, Mahalanobis distance [30] is used to drive the N_i, and a threshold ε_{mah} is chosen to construct a graph on all the point cloud samples, where the edge between v_i and v_j if and only if $d_{Mah}(v_i,\ v_j) < \varepsilon_{Mah}$.

However, not all cutting planes require rotational symmetries. For each vertex v_i in vasculature mesh, we should search for the best cutting plane φ_i^*. Specifically, the normal of φ_i^* should be most rotationally symmetric about the vertex normal in N_i. This problem can be solved iteratively, and Fig. 5 demonstrates this iteration process. We set an initial normal n_i^0, which satisfies $n_{cp}^0 \cdot n_i = 0$. Then the normal is iteratively update by

$$n_{cp}^{t+1} = arg\min \sum_{i=1}^{N} var\langle n_{cp}^t,\ n_i \rangle \tag{1}$$

where N is the size of N_i^t and N_i^t is the relevant neighbourhood at t-th iteration. n_i is the normal of vertex in N_i^t. $var\langle\cdot\rangle$ measures the angle between the vectors. By using singular value decomposition, Eq. 1 can be rewritten as one which minimizes the quadratic from $n_{cp}^T M n_{cp}$ with matrix

$$M = \begin{bmatrix} \overline{X^2} - \overline{X}^2 & 2\overline{XY} - 2\overline{X}\,\overline{Y} & 2\overline{XZ} - 2\overline{X}\,\overline{Z} \\ 2\overline{XY} - 2\overline{X}\,\overline{Y} & \overline{X^2} - \overline{X}^2 & 2\overline{YZ} - 2\overline{Y}\,\overline{Z} \\ 2\overline{XZ} - 2\overline{X}\,\overline{Z} & 2\overline{YZ} - 2\overline{Y}\,\overline{Z} & \overline{Z^2} - \overline{Z}^2 \end{bmatrix} \tag{2}$$

where X denotes a random variable for the x-component of the point normal in S, and $\overline{X}$ denotes the average of these x-components, similarly for Y, $\overline{Y}$, Z and $\overline{Z}$.

Next is to compute the position p_{cp}. The computed points collectively form the initial centerline point cloud. The

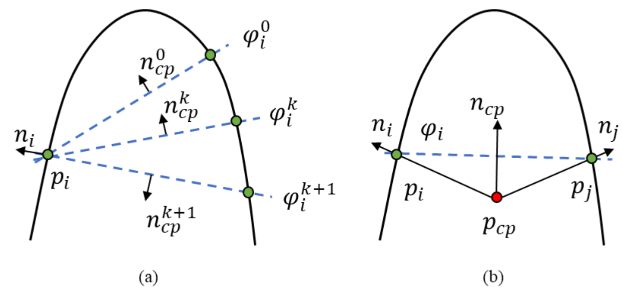

Fig. 5 2D illustration of iteration process. (a) The process for obtaining the best cutting plane. (b) When converging, the ROSA point (red point) is located at the intersection between p_i and p_j.

position p_{cp} is calculated by minimizing the sum of squared distances from p_{cp} to the normal lines.

$$p_{cp} = arg\min \sum_{i=1}^{N} \| (p_{cp} - p_i) \times n_i \|^2 \tag{3}$$

where $v_i = (p_i,\ n_i)$ is a vertex in N_i^* and N_i^* is the relevant neighbourhood for the best cutting plane φ_i^*, N is the size of N_i^*, and $(p_{cp} - p_i) \times n_i$ is the cross product of two vectors. Eq. 3 has a closed form solution by straightforward differentiation.

In the branch regions, the computed ROSA point is like a 1D structure, but the same does not hold for joints. Normally, the joint regions are not a cylindrical shape, thus it hasn't a meaningful optimal cutting plane. In order to maintain continuity, the Laplacian smoothing is used to connect the point from different branch regions. Moreover, the principal component analysis (PCA) is used to project ROSA point cloud onto their corresponding locally best-fitting lines. Before thinning the point cloud, we need to distinguish the ROSA point in the joint regions from those in the branches. Specifically, here use a standard linearity measure

$$\psi(c_i) = \frac{\lambda_i^{(1)}}{\lambda_i^{(1)} + \lambda_i^{(2)} + \lambda_i^{(3)}} \tag{4}$$

at a ROSA point c_i, where $\lambda_i^{(j)}$ is the j-th largest eigenvalue from the PCA at c_i. The thinning process uses 1D moving least squares (MLS) construction. When $\psi(c_i) < \xi_{MLS}$, it means that c_i is in a branch. In this research, the threshold ξ_{MLS} is set to 0.4. Finally, short curve segments method [31] is used to connect the samples to obtain a 1D curve skeleton.

C. *Pre-processing*

Traditional vascular-modeling methods reconstruct the vasculature mesh via extracting the vascular surface from volume images using the marching-cubes or skeleton-climbing algorithm [32]. The vasculature mesh is made up of tiny triangular planes. A vertex in vasculature mesh may be contained in different triangular planes. There exist two problems when we apply the centerline extraction method in vasculature mesh. One is that the vasculature mesh contains a lot of repetitive vertex, and the normal for repetitive vertex is different. These repetitive vertex does not increase accuracy but increase running time. Another problem is that the vasculature mesh is generally described as a closed entity rather than a hollow pipe. As a result, the end of the shape is a circular plane. The center point of this circular plane located at centerline of vasculature mesh. Therefore, this point will interfere with the centerline extraction method iterative searching for the ROSA points.

To solve these two problems, we propose a pre-processing method to deal the vasculature mesh before running the centerline extraction algorithm. Firstly, we measure the distance between the vertex to merge the repetitive vertex. If $d_e(v_i,\ v_j) < \varepsilon_e$, we combine v_i and v_j as one vertex, where $d(\cdot)$ is Euclidean distance and ε_e is the threshold. For each merged vertex, the normal is calculated by

$$n = norm\left(\sum_{i=1}^{N} n_i\right) \tag{5}$$

where N is the merged number for a vertex. $norm(\cdot)$ is normalization for the normal vector. Next, we detect the center point for a plane. If the normal for a vertex is always same, and the merged number for this vertex is large than threshold, we consider it is the center point for a circular plane. This vertex will be removed from the processed mesh.

III. Performance Evaluation

In this section, we assess the improved method on two vascular model to verify its performance. The experimental result is visualized. In addition, we compared the number of model vertex and running time after pre-processing.

A. Experimental Setup

We use two vascular model to verify the improved method. One is a bifurcated vessel model, as shown in Fig. 6 (a). Another is established based on the rigid vascular model, as shown in Fig. 7 (a). For visualization, the vascular model is made up of tiny triangular planes with red color.

The improved centerline extraction method is conducted in Matlab 2018b, and the computer is equipped with an Intel

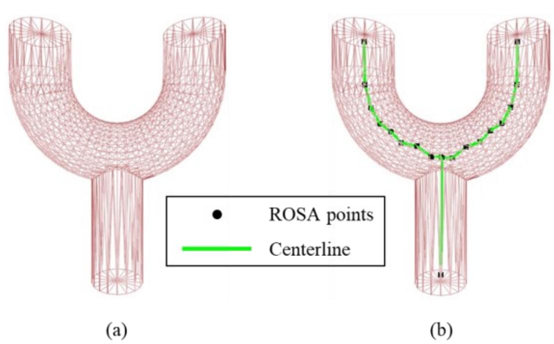

Fig. 6 The experiment in the bifurcated vessel model. (a) Visualization of the bifurcated vessel model. (b) Centerline extraction for the bifurcated vessel model. The ROSA points are visualized by black point and centerline is using green line.

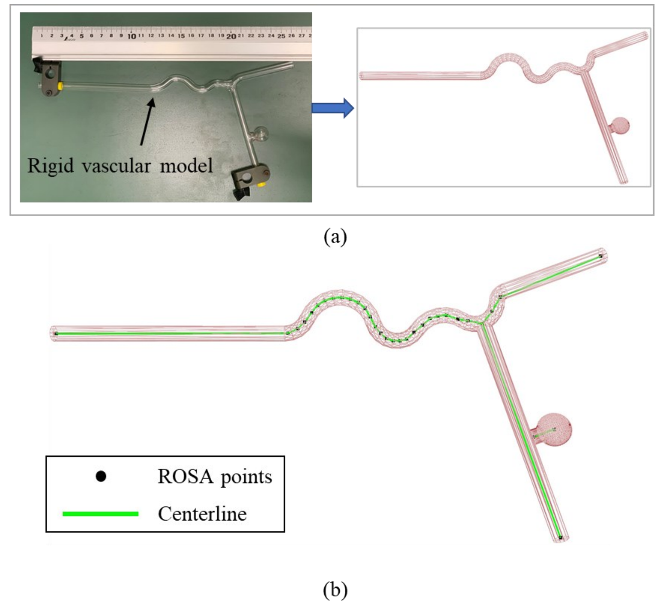

Fig. 7 The experiment in the rigid vascular model. (a) Visualization of the rigid vascular model. (b) Centerline extraction for the rigid vascular model. The ROSA points are visualized by black point and centerline is using green line.

TABLE I
Comparation of The Number of Model Vertex after Pre-processing

Vascular model	Vertex number	Vertex number*
Bifurcated vessel model	5.1 k	0.8 k
Rigid vascular model	9.2 k	1.5 k

* Pre-processed model

Core i7-8750H CPU with 16 GB memory, and an NVIDIA GeForce GTX 1060 GPU. The operating system is Windows 10. We use OpenGL to do the rendering task and the software is written in Python.

B. Experimental Result

The centerline extraction result for the bifurcated vessel model is shown in Fig. 6 (b), and Fig. 7 (b) is the result for the rigid vascular model. In the results, the black points are the extracted rotational symmetry axis points. The final centerline is visualized as green line. The results show that the improved centerline extraction method is sufficient to extract a complete centerline. However, it is nearly impossible to obtain a ground-truth centerline from a vasculature mesh. Therefore, we do not calculate the error of the extracted centerline. Our pre-processing method can effectively reduce the number of vertices while maintain the integrity of the vascular model. The comparation of the number of model vertex after pre-processing is shown in TABLE I.

IV. Conclusion

In this paper, we proposed an improved centerline extraction method based on generalized rotational symmetry axis. Our method assumes that the vasculature mesh is formed by a set of continuous cylindrical shapes. The centerline of vasculature is considered as a generalized rotational symmetry and the center point of each cylindrical shape is located at centerline. Due to rotational symmetry, the method can compensate for the missing data for vasculature mesh. To improve the operation efficiency, we proposed pre-processing strategy to merge duplicate vertices. Meanwhile, the plane normal vectors are converted to vertex normal vectors. Via the pre-processing strategy, the vasculature mesh is turned to vasculature point cloud. The experiment show that the improved centerline extraction method is sufficient to extract a complete centerline, and the pre-processing can effectively reduce the number of vertices while maintain the integrity of the vascular model.

Acknowledgment

This work was supported in part by the National High-Tech Research and Development Program (863 Program) of China under Grant 2015AA043202, and in part by SPS KAKENHI under Grant 15K2120.

References

[1] S. Guo et al., "A Novel Robot-Assisted Endovascular Catheterization System with Haptic Force Feedback," IEEE Transactions on Robotics, vol. 35, no. 3, pp. 685-696, 2019.

[2] X. Yin, S. Guo, N. Xiao, T. Tamiya, H. Hirata, and H. Ishihara, "Safety Operation Consciousness Realization of a MR Fluids-Based Novel Haptic Interface for Teleoperated Catheter Minimally Invasive Neurosurgery," IEEE/ASME Transactions on Mechatronics, vol. 21, no. 2, pp. 1043-1054, 2016.

[3] X. Bao, S. Guo, N. Xiao, Y. Li, and L. Shi, "Compensatory force measurement and multimodal force feedback for remote-controlled vascular interventional robot," Biomedical Microdevices, vol. 20, no. 3, p. 74, 2018.

[4] Y. Zhao et al., "A CNN-based prototype method of unstructured surgical state perception and navigation for an endovascular surgery robot," Medical & Biological Engineering & Computing, vol. 57, no. 9, pp. 1875-1887, 2019.

[5] C. Yang et al., "A vascular interventional surgical robot based on surgeon's operating skills," Medical & Biological Engineering & Computing, vol. 57, no. 9, pp. 1999-2010, 2019.

[6] L. Zheng, S. Guo. "A Magnetorheological Fluid-based Tremor Reduction Method for Robot Assisted Catheter Operating System" International Jou rnal of Mechatronics and Automation, vol.8, no.2, pp.72-79, 2020.

[7] L. Zhang et al., "Design and performance evaluation of collision protection-based safety operation for a haptic robot-assisted catheter operating system," Biomedical Microdevices, vol. 20, no. 2, p. 22, 2018.

[8] N. K. Sankaran, P. Chembrammel, A. Siddiqui, K. Snyder, and T. Kesavadas, "Design and Development of Surgeon Augmented Endovascular Robotic System," IEEE Transactions on Biomedical Engineering, vol. 65, no. 11, pp. 2483-2493, 2018.

[9] H. Rafii-Tari, C. J. Payne, and G.-Z. Yang, "Current and Emerging Robot-Assisted Endovascular Catheterization Technologies: A Review," Annals of Biomedical Engineering, vol. 42, no. 4, pp. 697-715, 2014.

[10] L. Zhang, S. Gu, S. Guo, and T. Tamiya, "A Magnetorheological Fluids-Based Robot-Assisted Catheter/Guidewire Surgery System for Endovascular Catheterization," Micromachines, vol. 12, no. 6. 2021, doi: 10.3390/mi12060640.

[11] H. Wang, J. Wu, and Y. Cai, "An adaptive deviation-feedback approach for simulating multiple devices interaction in virtual interventional radiology," Comput. Des., vol. 117, p. 102738, 2019, doi: https://doi.org/10.1016/j.cad.2019.102738.

[12] Y. Wang, F. Serracino-Inglott, X. Yi, X.-F. Yuan, and X.-J. Yang, "Real-time Simulation of Catheterization in Endovascular Surgeries," Comput. Animat. Virtual Worlds, vol. 27, no. 3–4, pp. 185–194, May 2016, doi: https://doi.org/10.1002/cav.1702.

[13] H. Blum, "A Transformation for Extracting New Descriptors of Shape," Models for the Perception of Speech and Visual Form, Proc. Symp., pp. 362-380, 1967.

[14] M. Schneider, S. Hirsch, B. Weber, G. Székely, and B. H. Menze, "Joint 3-D vessel segmentation and centerline extraction using oblique Hough forests with steerable filters," Med. Image Anal., vol. 19, no. 1, pp. 220–249, 2015, doi: https://doi.org/10.1016/j.media.2014.09.007.

[15] B. V Stimec, J. H. D. Fasel, and D. Ignjatovic, "3D Reconstruction of a Primary Aortoenteric Fistula – Centerline Calculation and Measurements," Current Medical Imaging Reviews, vol. 11, no. 2. pp. 127–131, [Online]. Available: https://www.ingentaconnect.com/content/ben/cmir/2015/00000011/00000002/art00011.

[16] A. Sharf, T. Lewiner, A. Shamir, and L. Kobbelt, "On-the-fly Curve-skeleton Computation for 3D Shapes," Comput. Graph. Forum, vol. 26, no. 3, pp. 323–328, Sep. 2007, doi: https://doi.org/10.1111/j.1467-8659.2007.01054.x.

[17] A. Tagliasacchi, H. Zhang, and D. Cohen-Or, "Curve Skeleton Extraction from Incomplete Point Cloud," ACM Trans. Graphics, vol. 28, no. 3, pp. 1-9, 2009.

[18] Y. Wang and T. Lee, "Curve-Skeleton Extraction Using Iterative Least Squares Optimization," IEEE Trans. Vis. Comput. Graph., vol. 14, no. 4, pp. 926–936, 2008, doi: 10.1109/TVCG.2008.38.

[19] O.K.C. Au, C. Tai, H. Chu, D. Cohen-Or, and T. Lee, "Skeleton Extraction by Mesh Contraction," Proc. ACM Siggraph, pp. 441- 449, 2008.

[20] M. Wei et al., "Centerline Extraction of Vasculature Mesh," IEEE Access, vol. 6, pp. 10257–10268, 2018, doi: 10.1109/ACCESS.2018.2802478.

[21] P. Shi, S. Guo, L. Zhang, X. Jin, H. Hirata, T. Tamiya and M. Kawanishi, "Design and Evaluation of a Haptic Robot-assisted Catheter Operating System with Collision Protection Function," in IEEE Sensors Journal, doi: 10.1109/JSEN.2021.3066424.

[22] X. Yin, S. Guo, H. Hirata, and H. Ishihara, "Design and experimental evaluation of a teleoperated haptic robot–assisted catheter operating system," J. Intell. Mater. Syst. Struct., vol. 27, no. 1, pp. 3–16, Nov. 2014, doi: 10.1109/JSEN.2021.3095187.

[23] Y. Song et al., "Performance evaluation of a robot-assisted catheter operating system with haptic feedback," Biomedical Microdevices, vol. 20, no. 2, pp. 50, 2018.

[24] P. Shi, S. Guo, X. Jin, and D. Song, "A Two-channel Haptic Force Interface for Endovascular Robotic Systems." in Proc. IEEE International Conference on Mechatronics and Automation (ICMA), pp.1602-1606, 2020.

[25] W. Zhou, S. Guo and Z. Chen, "A Novel Axial Force Feedback Device for the Master Manipulator of the Vascular Interventional Surgical Robot," 2020 IEEE International Conference on Mechatronics and Automation (ICMA), 2020, pp. 1631-1635.

[26] J. Guo and S. Guo, "Design and characteristics evaluation of a novel VR-based robot-assisted catheterization training system with force feedback for vascular interventional surgery," Microsyst. Technol., vol. 23, no. 8, pp. 3107–3116, 2017, doi: 10.1007/s00542-016-3086-x.

[27] B. Gao et al., "Construction of 3D vessel model of the VR Robotic Catheter System," in 2012 IEEE International Conference on Information and Automation, 2012, pp. 783–788, doi: 10.1109/ICInfA.2012.6246925.

[28] J. Guo and S. Guo, "A haptic interface design for a VR-based unskilled doctor training system in Vascular Interventional Surgery," in 2014 IEEE International Conference on Mechatronics and Automation, 2014, pp. 1259–1263, doi: 10.1109/ICMA.2014.6885880.

[29] J. Guo, S. Guo, T. Tamiya, H. Hirata, and H. Ishihara, "A virtual reality-based method of decreasing transmission time of visual feedback for a tele-operative robotic catheter operating system," Int. J. Med. Robot. Comput. Assist. Surg., vol. 12, no. 1, pp. 32–45, Mar. 2016.

[30] D. R. Pereira, J. P. Papa and A. N. Souza, "FEMaR: A finite element machine for regression problems," 2017 International Joint Conference on Neural Networks (IJCNN), 2017, pp. 2751-2757.

[31] J. Fan, E. D. Dottore, F. Visentin and B. Mazzolai, "Image-based Approach to Reconstruct Curling in Continuum Structures," 2020 3rd IEEE International Conference on Soft Robotics (RoboSoft), 2020, pp. 544-549.

[32] L. Schmid, M. Pantic, R. Khanna, L. Ott, R. Siegwart and J. Nieto, "An Efficient Sampling-Based Method for Online Informative Path Planning in Unknown Environments," in IEEE Robotics and Automation Letters, vol. 5, no. 2, pp. 1500-1507, April 2020.